Reversible Formation of Nanodomains in Monolayers of DPPC Studied by Kinetic Modeling

M. Stepanova*
National Institute for Nanotechnology, National Research Council of Canada, Edmonton, Alberta, Canada

ABSTRACT Dipalmitoylphosphatidylcholine (DPPC) is the most abundant component in pulmonary surfactants and is believed to be responsible for maintaining low surface tension in alveoli during breathing. In this work, a kinetic model is introduced that describes the phase separation in DPPC films that produces the liquid-condensed (LC) and liquid-expanded (LE) fractions, which differ according to the area density of DPPC. The phase separation in an initially homogeneous film has been investigated numerically. Furthermore, explicit simulations of periodic compression-expansion cycles are reported. In this process, a moderate change of the surface area resulted in a dramatic change in the total amount of LC fraction, as well as in the surface morphology. Depending on the extent of the film's compression, the simulated surface morphologies comprised individual nanosized LC domains embedded in the LE fraction, interconnected networks of such domains, or continuous LC films with nanopores. Equilibration of the total area of the LC nanodomains occurred over a few milliseconds, indicating that the rate of the LE-LC phase transformation is sufficient for maintaining low surface tension during breathing, and that nanoscale LC domains are likely to play a major role in this process. Unlike the total content of the LC fraction, which stabilized quickly, the average size of LC nanodomains showed a tendency to increase slowly, at a rate determined by the diffusivity of DPPC. The computed average domain size seems to be compatible with published experiments for DPPC films. The numeric results also elucidate the distinction between thermodynamically determined and kinetically limited structural properties during phase separation in the major structure-forming component of pulmonary surfactants.

INTRODUCTION

Self-assembled phospholipid films on the surface of a liquid form alveoli in lungs. The alveolar surfactant modulates the surface tension of the lung, stabilizes alveoli against collapse during expiration, and minimizes the work required to expand the alveoli during inhalation (1–3). To support these functionalities, the surfactant should be able to maintain a low surface tension and preserve its monolayer structure in wide regimes of surface pressures at physiological temperatures. On the other hand, a functional surfactant should also be able to adsorb rapidly at the air-liquid interfaces. It has been pointed out in the literature that these functionalities impose complementary requirements on the pulmonary surfactant: it should exhibit sufficient fluidity (flexibility) to rapidly distribute over the alveolar surface when its area changes and at the same time be structurally stable (solid) enough to resist collapse at high surface pressures and possess a structural organization that allows it to maintain a low surface tension under pressure by only a slight area reduction (1–3). The various components of the pulmonary surfactant, which are comprised of dipalmitoylphosphatidylcholine (DPPC), unsaturated lipids, cholesterol, and proteins, are supposed to support these complementary functionalities; however, neither the roles of each component nor the exact mechanisms involved are entirely clear to date. As emerges from experiments and existing model concepts, the pulmonary surfactant undergoes a reversible first-order phase transition in the process of breathing (1–3). At least two liquidlike phases are believed to be involved, which differ in their area density and level of molecular order (fluidity); in this article, these are denoted as the liquid-condensed (LC) and liquid-expanded (LE) phases. The corresponding morphological changes have been extensively studied by in vitro experiments through varying the surface area in model Langmuir-Blodgett films. Such experiments have revealed a reversible formation and dissolution of relatively rigid LC domains embedded in the LE phase, which has been adopted as a basic hypothetic mechanism through which the surfactant maintains a low surface tension and retains its structure under compression (1,2). However, the observed morphological changes were not always commensurate with this simple model. Thus, micron-sized LC domains (~10 μm) (4–7) were found to coexist with significantly smaller LC domains of nanocsale size (~10–100 nm) (8–16). Contrary to expectations, the area of micron-sized LC domains in the surfactant films sometimes remains largely unchanged or even decreases when the film is compressed (3,4,15,16). From such observations, an assumption has emerged that a reversible formation and dissolution of small nanoscale domains is in fact a major mechanism responsible for the function of the surfactant (3,10,15,16). This assumption seems to be supported by the fact that nanosized domains are observed systematically in various amphiphilic systems, including clinical surfactants (16), model mixtures of DPPC with unsaturated lipids (11,15), and films composed of DPPC (9,11–13).

DPPC, which is the most abundant component of pulmonary surfactants, is believed to play a central role in their

Submitted September 4, 2008, and accepted for publication March 23, 2009.

*Correspondence: maria.stepanova@nrc-cnrc.gc.ca

Editor: Reinhard Lipowsky.

0006-3495/09/06/4896/10 $2.00

doi: 10.1016/j.bpj.2009.03.041

structural organization. Apparently, DPPC is the only phospholipid that can form sufficiently rigid condensed phases for maintaining a monolayer structure when exposed to pressure at physiologically relevant temperatures (1–3) Indeed, in multicomponent surfactants, DPPC is the major constituent of LC domains, whereas other components are found mostly in the LE fraction and at the domain boundaries (2,3,13,16). The ability of DPPC to separate into distinctly different phases at physiological conditions is likely responsible for maintaining low surface tension during breathing (1–3). In contrast, unsaturated lipids (the second most abundant component, contained mostly in the LE fraction) seemingly enhance fluid properties of the surfactant when this is required (1,3,16). The role of other components, such as cholesterol and proteins, is even less clear, despite intense research (2,3,11,14–18).

Numerical modeling plays an important role in studies of the structure and function of biomembranes (19–22) To better understand the nanoscale organization of pulmonary surfactants, comprehensive models should be developed that describe the behavior of a mixture of the relevant components, as well as of monolayers containing pure DPPC. The latter case should even be addressed first, since DPPC is the most abundant component and seemingly responsible for the major functionality of the surfactant. Although other components also should be addressed, more complex mixtures cannot be adequately understood until a satisfactory model of pure DPPC is available. The challenge, however, is that there is a lack of comprehensive models capable of efficiently representing the detailed kinetic process of the LE-LC phase separation in either mixtures of different compounds or monolayers of pure DPPC. Part of the reason is that this fundamentally collective phenomenon requires both an accounting for atomic-scale interactions and handling of statistically large ensembles of interacting molecules at the same time. To reach a reasonable numeric efficiency, the intermolecular interactions are usually described by Lennard-Jones potentials or equivalent coarse-grained representations, which can only distinguish a difference in binding of the various components (say, DPPC and cholesterol and/or unsaturated lipids). As a result, most direct simulations of the surfactant's morphology as a function of time reported in the literature consider multicomponent membranes, where phase separation is driven simply by a difference in the short-distance bonds between molecules of different species (21,23–26). Although the basic theory of first-order phase transitions is very well elaborated (19), numerical studies capable of explicitly handling the detailed morphology changes during the phase separation in both mixtures and single-component membranes are rare (27–29).

This work reports an explicit kinetic modeling of the phase separation of LE-LC type in a single-component film representing a monolayer of pure DPPC. The corresponding intermolecular interaction accounts for both short-range and long-range forces, which are parameterized to describe the LE/LC phases in DPPC. In contrast to most existing numeric approaches, the model adopts a straightforward extension to include other components. However, this study focuses on the phase behavior of pure DPPC films, with the expectation that this behavior is of major importance for the function of the pulmonary surfactant. Evolution of nanoscale morphology in a film representing DPPC exposed to reversible compression/expansion cycles is described explicitly by kinetic modeling. The numeric results are discussed in detail and compared with published experiments.

METHODS

The time evolution of nanoscale morphologies in monolayers of DPPC undergoing a first-order phase transformation of the LE-LC type has been studied by mesoscopic kinetic modeling. In this model, the monolayer of DPPC is represented by the area density of the molecules, $\varphi(x, y, t) = \varphi(\vec{r}, t)$, which is a function of the coordinates, $\{x, y\} = \vec{r}$, and time, t. The evolution of density φ is described by the diffusion-drift equation (30,31)

$$\frac{\partial \varphi}{\partial t} = D\frac{\partial^2 \varphi}{\partial \vec{r}^2} - div\left(\frac{D}{kT}\varphi\frac{\partial \mu}{\partial \vec{r}}\right), \tag{1}$$

where D is the lateral diffusivity of DPPC in the monolayer, T is the temperature, $-\partial\mu/\partial\vec{r}$ is the mean force arising as a result of lateral intermolecular interactions, and μ is the chemical potential. The first term in the right-hand side of Eq. 1 describes diffusion, and the second term is associated with drift generated by the intermolecular interactions. The respective mean force, $-\partial\mu/\partial\vec{r}$, is given by (30)

$$-\frac{\partial \mu}{\partial \vec{r}} = h(\vec{r})\frac{\partial}{\partial \vec{r}}\int u(\vec{r} - \vec{r}')\varphi(\vec{r}')d\vec{r}', \tag{2}$$

where $u(r)$ is the effective pairwise potential describing intermolecular attraction at distance r, and the function $h(\vec{r})$ represents the impact of short-range intermolecular interactions. If the short-range interactions are disregarded ($h \equiv 1$), Eqs. 1 and 2 predict spontaneous formation of condensed domains where the density, φ, rises sharply (this behavior is also known as blow-up instability). The so-called effect of excluded volume, which accounts for intermolecular repulsion at short distances, can be introduced by requesting that $h(\vec{r})$ decrease from 1 for $\varphi(\vec{r}) << \varphi_C$ to 0 for $\varphi(\vec{r}) \geq \varphi_C$, where φ_C is density of the condensed phase (31). With the accounting for the effect of excluded volume, Eqs. 1 and 2 describe kinetics of the first-order phase transition of the vapor-liquid or vapor-solid type. In this case, domains of condensed phase coexist with a dilute 2D phase resembling vapor (30,31). However, this work addresses the phase transition between two liquid phases of different but comparable density. For both the LE and LC phases to acquire realistic densities, short-range attractive forces that are responsible for the continuity of the liquidlike membrane should be taken into account in addition to the effect of excluded volume. This can be achieved via the function $h(\vec{r})$:

$$h(\vec{r}) = \begin{cases} 0, & \varphi(\vec{r}) \leq \varphi_E; \\ 1, & \varphi_E < \varphi(\vec{r}) < \varphi_C; \\ 0, & \varphi(\vec{r}) \geq \varphi_C. \end{cases} \tag{3}$$

Here, φ_C is the density of the LC phase and φ_E is the density of the LE phase. When Eq. 3 is employed for $h(\vec{r})$ in Eq. 2, the drift due to the long-range attraction occurs only under the condition where the local density, $\varphi(\vec{r})$, is $<\varphi_C$ but $>\varphi_E$. This prevents the density from exceeding these limits spontaneously, and can be understood as the outcome of the short-range forces of

intermolecular repulsion and attraction, which are responsible for the effect of excluded volume and the film's continuity, respectively. The assumed aptitude of the short-range repulsive and attractive forces to override the long-range attraction when the density exceeds the limits given, reflects the well known fact that the short-range forces are significantly stronger than those described by the long-range potential, u.

In this work, the conditions of excluded volume and film continuity are accommodated through the an approximation for the function $h(\vec{r})$:

$$h(\vec{r}) = \begin{cases} 0, & \varphi(\vec{r}) \le \varphi_E; \\ \left(1 - \left(\frac{\varphi_E}{\varphi(\vec{r})}\right)^n\right)\left(1 - \left(\frac{\varphi(\vec{r})}{\varphi_C}\right)^n\right); & \\ 0, & \varphi(\vec{r}) \ge \varphi_C \ . \end{cases} \quad (4)$$

Tests have shown that the results of modeling are largely insensitive to the power n for $n > 4$. In this article, $n = 10$ is employed. The densities of LE and LC phases of DPPC, φ_E and φ_C, are chosen to match the experimentally determined surface areas/molecule of 55 Å^2 and 80 Å^2, respectively (5,27,32).

The pairwise potential, $u(r)$, is asymptotically given by

$$u(r) \approx -kTC(r), \quad r \to \infty, \quad (5)$$

where $C(r)$ is the long-range part of the direct correlation function of DPPC molecules (33).The head-to-head direct correlation function for DPPC molecules, which has been estimated using the basic theory of molecular solvation, and which is also known as the reference interaction site model (1D-RISM) (34,35), is shown in Fig. 1. Here, the long-range part of the function $C(r)$ is approximated by

$$C_{\text{appr}}(r) = C_0\left[\frac{r_2 - r}{r_1} + \sqrt{1 + \left(\frac{r_2 - r}{r_1}\right)^2}\right], \quad (6)$$

where $C_0 = 4.88 \times 10^{-2}$, $r_1 = 2.0$ nm, and $r_2 = 6.3$ nm. Fig. 1 demonstrates that this approximation provides a very good fit for $r \ge 1.7$–1.8 nm. For shorter distances, the function $C(r)$ is not considered in detail, because in this model, the short-range interactions have already been accounted for through the function $h(\vec{r})$. According to numerical tests, the choice of $C_{\text{appr}}(r)$ at short distances does not influence the results significantly, at least for a single-component system. In this article, C_{appr} is obtained by extrapolating Eq. 6 toward short distances, as shown in Fig. 1.

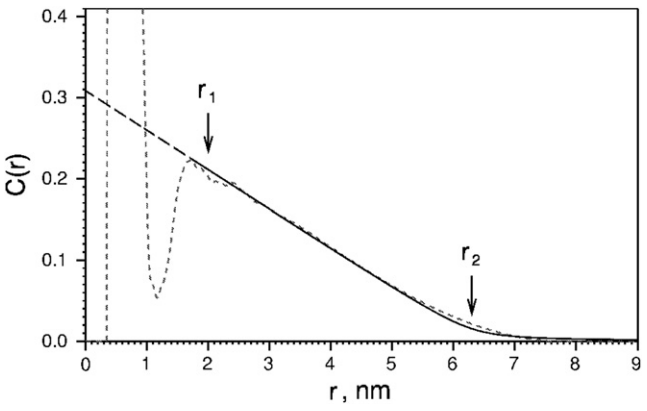

FIGURE 1 Head-to-head direct correlation function, $C(r)$, for DPPC: RISM (*short-dashed line*), Eq. 6 (*solid line*), and extrapolation of Eq. 6 toward short distances (*long-dashed line*). The RISM head-to-head direct correlation is courtesy of L. Livadaru, who generated the function through the self-consistent molecular theory of polymer melts and solutions employing the basic reference interaction site model (1D-RISM (34,35)). $C(r)$ represents the head-to-head correlation after equilibration of a mixture of DPPC molecules and water, with the average intermolecular distance corresponding to the LE phase.

The lateral diffusivity, D, of phospholipids in amphiphilic membranes is not known precisely; experiments indicate that the order of magnitude may range from ~0.01 to ~1 μm^2/s at room temperature (36–39). In this work, the diffusivity, D, varied within the limits determined experimentally. On the basis of these assumptions, Eq. 1 was solved numerically in a 2D rectangular area adopting periodic boundary conditions.

RESULTS

Fig. 2 shows the simulated evolution of the nanoscale morphology for an initially uniform distribution of DPPC molecules. The initial average concentration $\overline{\varphi_{\text{init}}}$ was chosen to fall within the region of the LE-LC phase coexistence, $\overline{\varphi_{\text{init}}} = 0.6\varphi_{\text{E}} + 0.4\varphi_{\text{C}}$, which corresponds to a 40% area coverage of the LC fraction. A slight random fluctuation was added over this uniform background to provide the initial morphology shown in Fig. 2 *a*. Fig. 2, *b*–*d*, demonstrates that nanosized domains of the condensed phase (represented by dark spots) self-assemble spontaneously.

It should be especially emphasized that the initial distribution in Fig. 2 *a* represents a single-component system, and not a mixture of some LE and LC components, as most existing models assume. Throughout this article, the LC and LE phases are identified uniquely according to the local

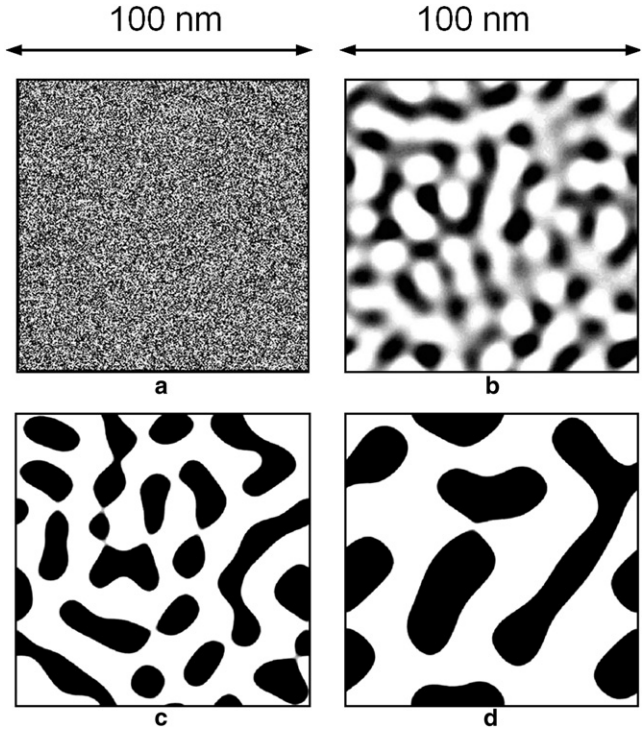

FIGURE 2 Spontaneous separation of a homogeneous distribution (*a*) into the LC phase (*dark spots*) and the LE phase (*light background*) at 0.05 ms (*b*), 0.5 ms (*c*), and 5 ms (*d*). In this example, the diffusivity $D = 0.1$ μm^2/s was used. The size of the film was 100 × 100 nm. The initial concentration of DPPC molecules corresponded to a 40% LC coverage at equilibrium.

density adopted by the single-component film, without any distinguishing between molecules in the LE and LC phases. Accordingly, the results given below adequately represent first-order phase separation of the LE-LC type in a single-component system.

Fig. 2 shows that formation of the LC domains out of the uniform distribution occurs quite rapidly. After 0.5 ms, well shaped domains of the condensed phase are already available. The overall area of the LC fraction reaches the equilibrium level of ~40% by this stage, and remains stable in the stages that follow. However, the average size of the nanodomains keeps increasing after the total content of the LC fraction has stabilized (see Fig. 3). This coarsening includes two basic mechanisms, one of which is known as Ostwald ripening (29), and can be compared to evaporation-condensation that results in a growth of large LC domains at the expense of the dissolution of small ones. Coalescence (merging) of nanodomains is another mechanism leading to coarsening of the nanoscale structure. As can be seen in Fig. 3, coarsening of nanodomains depends on the diffusivity, D. A stronger diffusion results in a smaller number of larger LC domains at a given time, which can be represented by the power-law expression for the average domain size, $L \sim (Dt)^{0.41}$. In contrast to the fast process of equilibration of the total area of the domains, the increase of their average size is slow and virtually unlimited unless the film is stretched so that a new equilibration process is started.

Fig. 4 demonstrates the change of morphology in a hypothetic model process, where a phase-separated film is stretched slightly, increasing the surface area by 15%. Fig. 4 *a* shows the initial morphology in the uniformly stretched phase-separated film, Fig. 4, *b–d*, demonstrates the subsequent process of equilibration, and Table 1 (*upper row*) presents the respective change in the percentage of the LC fraction. It is clearly seen that the total area of LC domains decreases during ~3 ms, when the amount of the LC fraction approaches the new equilibrium level. Compression of a phase-separated film results in a rapidly increasing amount of the LC fraction over a millisecond time interval, after which the area fraction of the condensed phase stabilizes (Table 1, *lower row*). Comparison of the results given in Table 1 shows that in the compressed film, the equilibration of the amount of LC phase occurs faster than in the stretched one. The reason is that LC nanodomains can nucleate out of the compressed LE fraction in addition to the growth of existing LC domains, which accelerates the process of equilibration. Fig. 5 demonstrates the time required to equilibrate the total area of the LC fraction, τ, as a function of the lipid diffusivity D. The dependence shown in Fig. 5 follows from Eq. 1, according to which the entire model can be represented as a function of the

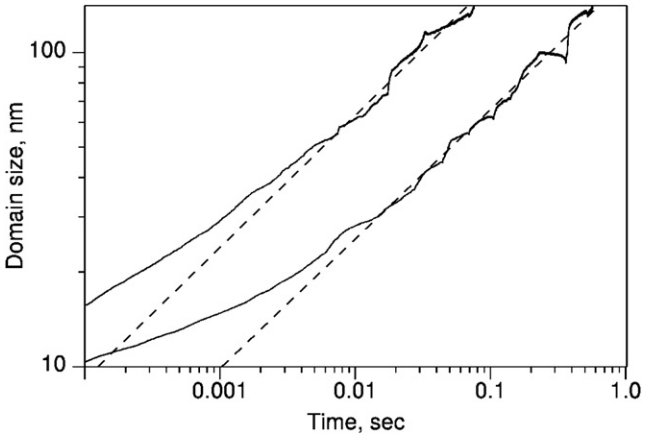

FIGURE 3 Average size of LC domains as a function of time for $D = 0.1\ \mu m^2/s$ (*lower curve*) and $D = 1\ \mu m^2/s$ (*upper curve*). The results of modeling are indicated by solid lines, and the empiric asymptotic dependence, $L = 430(Dt)^{0.41}$, by dashed lines, where L is given in nm, D in $\mu m^2/s$, and t in s. The size of the film was 200 × 200 nm, and the equilibrium LC coverage was equal to 40%.

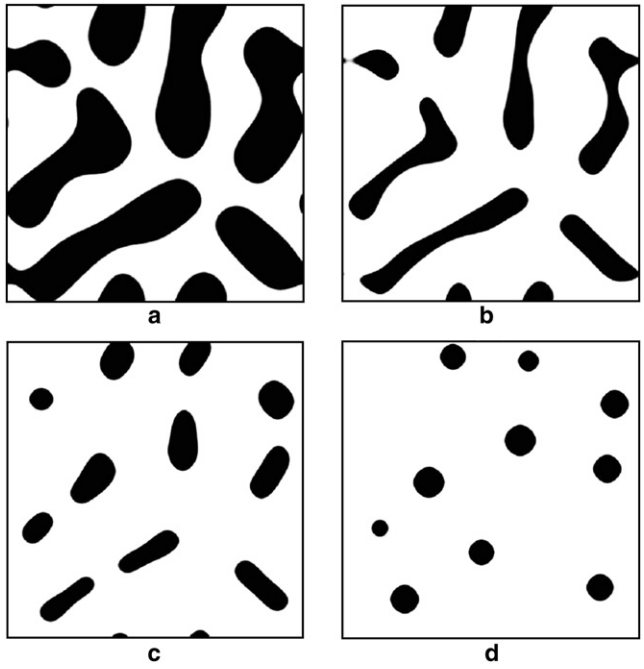

FIGURE 4 Equilibration of the morphology after a hypothetic stretching of a phase-separated film, showing the phase-separated morphology after a 15% area increase initially (*a*), and after 0.05 ms (*b*), 0.5 ms (*c*), and 5 ms (*d*) The diffusivity, D, was equal to 0.1 $\mu m^2/s$. The size of the film was 85 × 85 nm before stretching and 100 × 100 nm after stretching, and the equilibrium concentration was 46% before stretching and 7% after stretching.

TABLE 1 Percentage of LC phase at various equilibration times in a hypothetic stretched film and compressed film

Time (ms)	0	0.05	0.5	1	2	3	4	5
Stretched film, % of LC fraction	46	24	15	12	9	8	8	8
Compressed film, % of LC fraction	7	40	44	45	46	46	46	46

In the stretched film (*upper row*), the initial content of the LC fraction was 46%, and the equilibrium content was 7%. In the compressed film (*lower row*), the initial content of the LC fraction was 7%, and the equilibrium content was 46%.

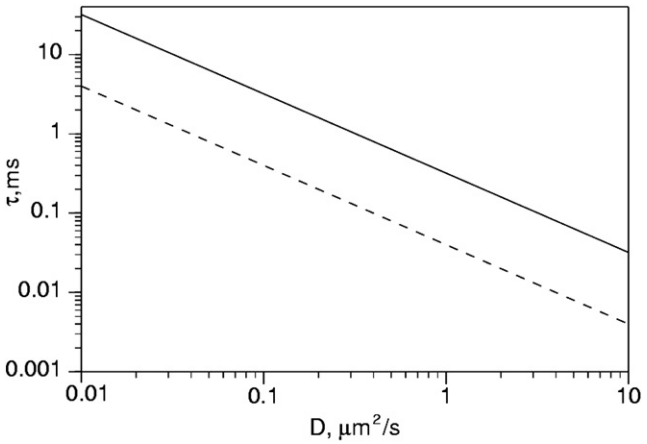

FIGURE 5 Time τ required to equilibrate the total area of the LC fraction as a function of the diffusivity, D, after extension (*solid line*) and compression (*dashed line*) of the film.

variable, Dt. This leads to the corresponding inverse proportionality $\tau \sim D^{-1}$ seen in Fig. 5.

Fig. 6, *a–d*, demonstrates the morphology in a phase-separated film whose surface area sequentially increases and decreases. It can be seen that both the size and surface area of the LC domains change reversibly. The equilibration time of only 2 ms considered in this hypothetic process seems to be sufficient to accommodate the reversible change in the content of the LC fraction. Thus, the content of the LC fractions in Fig. 6, *b* and *d*, has reached the equilibrium level of 46%, and that in Figs. 6, *a* and *b*, is equal to 9%, which is close to the equilibrium value of 7%. Fig. 6, *e–h*, illustrates a similar periodic process, with the equilibration time of 20 ms. It can be seen that the LC domains in Fig. 6, *e–c*, are larger than those in Fig. 6, *a* and *b*. which is related to a more pronounced coarsening of the domains over the longer compression-expansion cycle (see also the dependencies of the domain size on time in Fig. 3). In contrast, the total content of the LC fraction is not sensitive to the increase of the equilibration time from 2 to 20 ms.

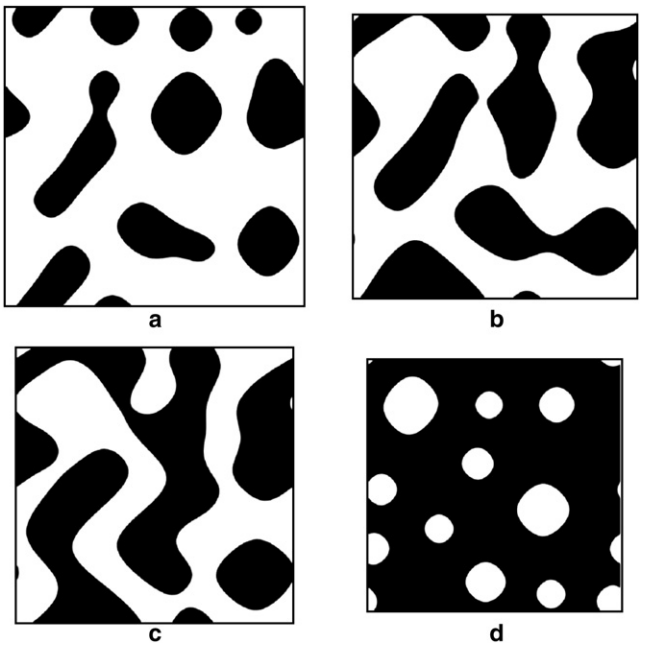

FIGURE 7 Nanoscale morphologies at 5 ms after compression of a film initially containing 7% of the LC fraction with the area reduced by 10% (*a*), 15% (*b*), 17% (*c*), and 25% (*d*).

Figs. 7 and 8 illustrate the dependence of the surface morphology on the area reduction. Thus, Fig. 7, *a–d*, presents the morphologies that develop in 5 ms after area reduction by 10%, 15%, 17%, and 25%, respectively, of an initial film containing 7% of the LC phase. Fig. 8 shows the corresponding total LC coverage as a function of the area reduction. The dependence in Fig. 8 can be represented by the expression

$$c_{\mathrm{LC}} = \frac{c_{\mathrm{LC}}^0}{1-x} + \frac{x}{1-x}\frac{\varphi_{\mathrm{E}}}{\varphi_{\mathrm{C}} - \varphi_{\mathrm{E}}}, \tag{7}$$

which follows from simple arguments based on the Maxwell rule for equal areas. Here, c_{LC}^0 and c_{LC} are equilibrium

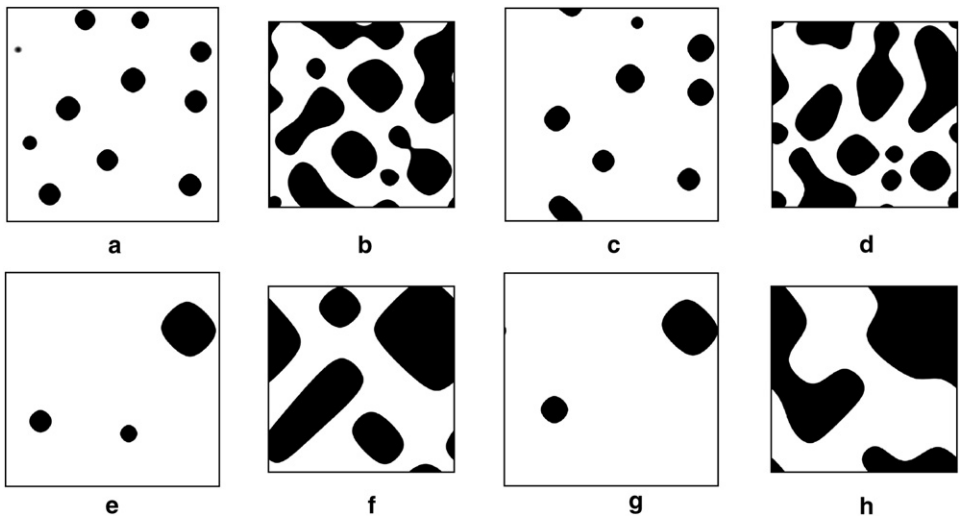

FIGURE 6 Reversible change of morphology during a hypothetic process, where the area of the film sequentially increases and decreases. Equilibration times were 2 ms (*a–d*) and 20 ms (*e–h*), and film sizes were 100 × 100 nm (*a*, *c*, *e*, and *g*) and 85 × 85 nm (*b*, *d*, *f*, *h*). The diffusivity $D = 0.1\ \mu\mathrm{m}^2/\mathrm{s}$ was used.

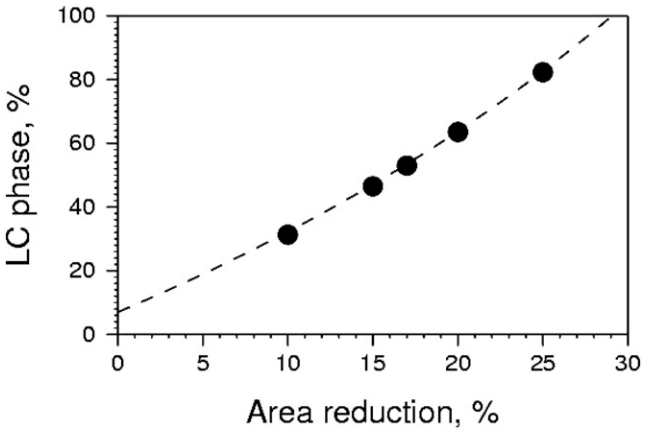

FIGURE 8 Total percentage of the LC fraction as a function of the relative area reduction for an initial LC coverage of 7%. The points represent modeling with 5-ms equilibration and the line represents Eq. 7.

fractions of the LC phase before and after compression, respectively, φ_E and φ_C are the area densities in the LE and LC phases, and x is the relative area reduction, $x = (A_0 - A)/A_0$, where A_0 and A are the areas before and after compression, respectively.

The fraction of the LC phase after compression determines the morphology in the film. As can be seen in Fig. 7, nanodomains of the LC phase embedded in the LE phase are formed when the LC coverage is <50% (Fig. 7, *a* and *b*). When LC coverage is close or slightly higher than 50%, the domains develop an interconnected network (Fig. 7 *c*). At higher compression, an LC film is formed that contains islands (pores) filled with LE fraction, as illustrated in Fig. 7 *d*.

DISCUSSION

In line with published experiments and theoretical predictions (2,3,19), the kinetic model introduced here shows a clear phase separation as a result of the first-order phase transformation ''liquid-liquid'' in a single-component film representing a monolayer of DPPC. This process generates nanoscale LC domains embedded in the LE phase (Fig. 2). With time, the LC nanodomains tend to coarsen, e.g., increase in size, whereas their number decreases.

The explicit simulation of the repeating compression-expansion cycles (see Fig. 6) has shown reversible changes of both the total content of the LC fraction and the morphology of the nanodomains. Expansion leads to dissolution of LC domains, whereas compression generates both growth of existing LC domains and nucleation of new ones. Both dissolution and precipitation of the LC fraction are found to be fast processes. Equilibration of the total area of LC nanodomains may occur over a few milliseconds, or even shorter times, for both dissolution and expansion (see Table 1 and Fig. 5), which agrees with the recent theory for phase separation in bilayers (29). The characteristic time of the phase separation is significantly less than most physiologically relevant time regimes, indicating that the rate of the LE-LC phase separation is sufficient to support the hypothetic functionality of DPPC, which is to maintain low surface tension when the area of the surfactant changes. The high rate of phase separation in comparison to the physiologic time regimes indicates that the major function of DPPC in pulmonary surfactants is rather thermodynamically determined, whereas kinetic factors may play a less important role in this functionality.

According to the Maxwell rule, the equilibrium amount of the LE and LC fractions is determined by the average area density of DPPC molecules. As a result, compressing or stretching a phase-separated film induces changes of the relative content of LC and LE fractions (Figs. 4, 6, and 7). Thus, compression leads to an increase of the total amount of the LC fraction contained in nanodomains (Figs. 7 and 8), in agreement with recent experimental observations (15,16). It is worth remarking that a moderate decrease in the surface area of the film (by 25–30% or less) results in significant changes in the cumulative LC coverage, as it is evident from Fig. 8 and Eq. 7. Equation 7 predicts that for a small area reduction ($x << 1$), the content of LC fraction φ_{LC} increases roughly in proportion to x, $c_{LC} \approx c^0_{LC} + x\frac{\varphi_E}{\varphi_C - \varphi_E}$. The sensitivity of c_{LC} to the compression is determined by the coefficient $\frac{\varphi_E}{\varphi_C - \varphi_E}$, which is equal to ~2.2 for DPPC. Thus, an area reduction of 15% results in a 33% increase of the content of LC fraction. At higher compressions x, the increase of c_{LC} with x becomes even stronger. A compression leading to $c_{LC} = 1$, which corresponds to a 100% LC coverage, is the maximum area reduction at which the film is capable of maintaining its monolayer structure. This maximum area reduction is given by $x_{max} = (1 - c^0_{LC})\frac{\varphi_C - \varphi_E}{\varphi_C}$. For DPPC, assuming $c^0_{LC} = 0$, the maximum achievable compression is ~31%, which is consistent with the variation of alveolar surface area during breathing. Further compression beyond x_{max} should result in the film folding or collapsing with the formation of multilayers, or other 3D structures allowing a release of the excess deformation (1–3).

The relative amounts of LE and LC phases determine the shape of the LC nanodomains, which changes from individual spots at moderate LC coverage (Fig. 7, *a* and *b*) to networks of interconnected nanodomains when the LC coverage exceeds 50% (Fig. 7 *c*). In each case, the emerging morphology minimizes the length of the LE-LC interphase boundaries for a given total amount of the LC fraction and average size of the domains available in the system. There is a noticeable similarity between the numeric results and the experimentally detected morphology of the nanodomains (11,12,15,16). A stronger compression leads to merging of the nanodomains into a nearly continuous LC film with nanopores containing LE fraction (Fig. 7 *d*), reminiscent of experimentally observed morphologies within large, micron-sized domains (2,11,12,15,16) This observation

seems to support the recent hypothesis that micron-sized LC domains may be formed by merging of nanodomains (11,15). Considering that the content of the LC phase is determined by the average area density of DPPC molecules, one can further assume that merging occurs at locations where the average area density of DPPC is increased, e.g., by fluctuations and/or as a result of transient processes of the surfactant's redistribution over the varying surface area. The merging hypothesis may explain the absence of a clear correlation between the number of large, micron-sized domains and the film's compression, detected in some experiments (3,4,15,16).

Unlike the total area occupied by the LC nanodomains and their shape, which stabilize quickly, the average size of the domains tends to increase slowly, and their number decreases accordingly (see Figs. 2 and 3). From general theory (19), it is known that this coarsening is a thermodynamically driven process, which decreases the length of the LE-LC interphase boundaries at a given LC coverage. The numeric results shown in Figs. 2, 3, and 6 demonstrate that the average size of LC nanodomains indeed depends on the time of the film's equilibration. Thus, the domain size and the related structural properties, e.g., the number of the domains and the total length of the LE-LC interphase boundaries, emerge as the kinetically determined structural properties.

From the model simulations represented by Fig. 3, the average size of DPPC domains can be approximately described by the dependence

$$L = 340(Dt)^{0.41}, \quad (8)$$

where L is measured in nm, D in $\mu m^2/s$, and t in s. Table 2 presents the corresponding sizes of LC domains for selected time regimes and various diffusivities, D. Thus, after a typical time period required for the LC content to equilibrate, the domain size ranges from a few nanometers to a few tens of nanometers. Over half of the respiration cycle, the domains can grow up to tens to hundreds of nanometers. Equilibration times from minutes to one hour, which are typically reached during in vitro experiments, may lead to micron-sized LC domains. The latter prediction is compatible with experiments for pure DPPC films, where LC domains sized from 400–500 nm (11,12) to 1–2 μm (13) were observed. Indeed, from Table 2 and Eq. 8, it follows that according to the model presented here, a 10- to 30-min equilibration leads to 500-nm to 1-μm domains for diffusivities of $D = \sim 0.01\ \mu m^2/s$.

TABLE 2 Computed average size of LC domains, for various diffusivities and selected time regimes

	Average domain size, L (nm)			
Time	$D = 0.01\ \mu^2/s$	$D = 0.1\ \mu^2/s$	$D = 1\ \mu^2/s$	Comments
3 ms	4	16	40	Equilibration of total LC content
2 s	86	220	570	Half respiration cycle (humans)
10 min	900	2,300	5,900	In vitro experiments
60 min	1,900	4,700	12,000	In vitro experiments

In contrast to pure DPPC, nanodomains observed in multicomponent surfactants are systematically smaller than predicted numerically for comparable equilibration times. Thus, experiments with clinical surfactants (14,16) and model mixtures of DPPC with other lipids, cholesterol, and membrane proteins (11,13,15) show that ~10-μm LC microdomains coexist with nanodomains with an average size from 60 to 250 nm after ~30 min to ~1 h of equilibration. This resistance of nanodomains to coarsening, which seems to contradict the expectations for a phase-separating system, has been addressed by many authors (12,13,15,29,17,18). It was suggested that growth of LC domains may be obstructed by their interaction with other compounds in the LE fraction, leading to a decrease in the interphase line tension (29). The latter hypothesis seems to agree with experiments in which the addition of cholesterol or proteins SP-A or SP-B resulted in smaller and more numerous nanodomains (11,14–16). Another explanation emerging from this study is that the slowing down of the domain coarsening in surfactants may also originate from the damping impact of some compounds, e.g., cholesterol (37), on the diffusivity of DPPC molecules. Fig. 3, Table 2, and Eq. 8 demonstrate that a decrease in diffusivity leads to a decrease in the average size of domains in proportion to $\sim D^{0.41}$. Thus, LC domains with the average size of ~100 nm after a 10-min equilibration could result from DPPC diffusivities of $\sim 0.5 \times 10^{-4}\ \mu m^2/s$. The diffusivity of DPPC molecules discussed here should not be confused with the fluidity of the surfactant, which is enhanced in the presence of unsaturated lipids and, apparently, cholesterol (1–3). In contrast, the molecular diffusivity potentially can be damped in the presence of those compounds. The alternative mechanism would assume attachment of cholesterol or protein molecules to the boundaries of LC domains (2,18). If this attachment is capable of decreasing the boundary line tension, then the domains can be stabilized, resulting in a larger number of smaller domains (14,15,29). Future inclusion in the model of components other than DPPC, and corresponding numeric studies, will clarify exactly what mechanism results in the observed stabilization of the domain size in multicomponent surfactants.

In the methodological context, this article introduces a basic model that explicitly describes the kinetic process of the nanoscale morphology evolution as a result of the first-order phase transition ''liquid-liquid'', demonstrates its capacity in the light of published experimental observations, and outlines further research needs. The specific material (DPPC) is accounted for by the parameterization of the model, employing the equilibrium densities of the LE and LC phases, φ_E and φ_C, the long-range intermolecular potential, $u(r)$, and the surface diffusivity, D. These material parameters differ significantly in the level of precision at which they are available, as well as in the robustness of

the model with respect to possible uncertainties. Thus, the model is sensitive to the equilibrium densities, φ_E and φ_C, which, however, are quite well known from experiments. It is important for the long-range intermolecular attraction, $u(r)$, to exist at distances of ~2–4 nm. However, the model has shown a significant robustness with respect to the particular details of the profile $u(r)$, provided that the level of u is a reasonable order of magnitude (~kT or less). This robustness has made it possible to employ the head-to-head correlation function from the basic 1D-RISM model (34,35) to estimate $u(r)$. A more precise definition of $u(r)$ would require a development of the 3D-RISM simulation (40,41) for a monolayer of DPPC at the air-water interface. This allows complementing the kinetic model with a more rigorous determination of the long-range intermolecular potential of attraction. Another point that should be clarified is the lateral diffusivity of DPPC molecules in the monolayer. From experiments, it can be seen that the diffusivity may vary significantly (36–39), allegedly because of its dependence on the local density and composition in the layer. Including the dependence of diffusivity on density, resulting in different diffusivities in the LE and LC phases, presents another possibilitly for future improvement of the model. In regard to new biophysical effects to consider, extension of the model to handle mixtures of various lipids, cholesterol, and proteins should be the next major step. Equation 1 per se would adopt such an extension rather simply, but the corresponding parameterization would require a number of methodological inventions. Another point, the importance of which is addressed increasingly in the literature, is the possible formation of 3D multilayer structures in lung surfactant. Although multilayer mesophases are not a part of this model, their formation could be accounted for effectively, e.g., by including sinks of the surfactant near the boundaries of large LC domains. In this light, this introductory study can be considered as the background for a wide range of more detailed studies in the future, including the effects of collapse and formation of multilayers in the alveolar surfactant.

SUMMARY

The numeric results described in this study represent the phase separation in monolayers of pure DPPC, resulting in well separated nanostructured LC and LE fractions, which differ according to the area density of the lipid. Depending on the average number of DPPC molecules/unit area, the phase separation generates individual nanosized LC domains embedded in the LE fraction, interconnected networks of such domains, or continuous LC films with nanopores containing LE fraction. In each case, the morphology minimizes the length of the LE-LC interphase boundaries. The shape of the simulated morphologies resembles closely the nanoscale organization of amphiphilic surfactants observed experimentally.

Reversible precipitation-dissolution of LC nanodomains has been studied by an explicit simulation of periodic compression-expansion cycles. In agreement with published experiments, moderate changes of the surface area of a phase-separated film result in a dramatic impact on the cumulative area occupied by LC nanodomains. Both dissolution and precipitation of the LC fraction are fast processes that occur over short times of a few milliseconds. The characteristic time of the equilibration of the total LC content is significantly less than most physiologically relevant time regimes, indicating that the rate of the LE-LC phase separation is sufficient to accommodate the reversible response of the total amount of the LC fraction to changes of the surface area during breathing. After equilibration, the cumulative area of LC nanodomains is directly related to the extent of the film's compression or expansion. These results seem to support the recent hypothesis that the dominant role of the LC nanodomains is to maintain the low surface tension in alveolae (3,15,16). As concerns the large, micron-scale LC domains, the numeric results presented here confirm that these structures may arise from an aggregation of nanodomains in locations where the area density of DPPC is increased (11,15). The aggregation hypothesis may explain the absence of a direct correlation, detected in some experiments (3,4,15,16), between the micron-scale domains and the film's compression.

In contrast to the total content of the LC fraction, which stabilizes quickly, the average size of LC nanodomains shows a tendency to increase slowly, whereas their number decreases accordingly. The rate of this coarsening is determined by the diffusivity of DPPC molecules, and the average size of the nanodomains is limited by the equilibration time of the film. The average size of LC domains detected experimentally in DPPC films (11–13) seems to be compatible with model predictions.

Unlike DPPC films, nanodomains observed experimentally in multicomponent surfactants (11,13,14,16,15) are systematically smaller than predicted numerically. In addition to the presumably stabilizing attachment of cholesterol or protein molecules to the boundaries of LC domains (2,14,15,29,18), another emerging explanation is that the slowing down of the coarsening might result from a low diffusivity of DPPC molecules in multicomponent surfactants. Further numeric studies will clarify what mechanism is responsible for the observed stabilization of the nanodomains in compound surfactants.

Overall, this numeric study has clarified the distinction between thermodynamically determined properties and kinetically limited processes in DPPC films. Thus, the total amount of the LC fraction contained in the nanodomains and their mesoscopic aggregates is shown to be thermodynamically determined. The nanoscale organization (individual LC domains, interconnected networks, or porous aggregates) appears to be thermodynamically determined as well. In contrast, the size of the nanodomains, their

number per unit area, and the corresponding total length of the LE-LC interphase boundaries are rather kinetically limited. These properties depend on the molecular diffusivity, equilibration time, and, particularly for multicomponent surfactants, the presence of additional damping or obstructive mechanisms that may limit coarsening of the nanoscale structure. This study is critical for a better understanding of the function of the major component of pulmonary surfactants, and it also demonstrates the potential of the kinetic model to describe quantitatively the phase behavior of DPPC membranes. The model is easily upgradeable to include components other than DPPC and may serve as a background for future theoretic developments.

The head-to-head direct correlation function for DPPC molecules given in Fig. 1 was provided by L. Livadaru and A. Kovalenko, who generated the function $C(r)$ using the theory of molecular solvation (34,35).

This work was supported by the National Research Council of Canada.

REFERENCES

1. Piknova, B., V. Schram, and S. B. Hall. 2002. Pulmonary surfactant: phase behavior and function. *Curr. Opin. Struct. Biol.* 12:487–494.
2. Wüstneck, R., J. Perez-Gil, N. Wüstneck, A. Cruz, V. B. Fainerman, et al. 2005. Interfacial properties of pulmonary surfactant layers. *Adv. Colloid Interface Sci.* 117:33–58.
3. Zuo, Y. Y., R. A. W. Veldhuizen, A. W. Neumann, N. O. Petersen, and F. Possmayer. 2008. Current perspectives in pulmonary surfactant: inhibition, enhancement, and evaluation. *Biochim. Biophys. Acta.* 1788: 1947–1977.
4. Nag, K., J. Perez-Gil, M. L. F. Ruano, L. A. D. Worthhmann, J. Stewart, et al. 1998. Phase transitions in films of lung surfactant at the air-water interface. *Biophys. J.* 74:2983–2995.
5. Discher, B. M., K. M. Maloney, D. W. Grainger, C. A. Sousa, and S. B. Hall. 1999. Neutral lipids induce critical behavior in interfacial monolayers of pulmonary surfactant. *Biochemistry.* 38:374–383.
6. Discher, B. M., W. R. Schief, V. Vogel, and S. B. Hall. 1999. Phase separation in monolayers of pulmonary surfactant phospholipids at the air-water interface: composition and structure. *Biophys. J.* 77:2051–2061.
7. Alonso, C., T. Alig, J. Yoon, F. Bringezu, H. Warriner, and J. A. Zasadzinski. 2004. More than a monolayer: relating lung surfactant structure and mechanics to composition. *Biophys. J.* 87:4188–4202.
8. Chi, L. F., M. Anders, H. Fuchs, R. R. Johnston, and H. Ringsdorf. 1993. Domain structures in Langmuir-Blodgett films investigated by atomic force microscopy. *Science.* 259:213–216.
9. Hollars, C. W., and R. C. Dunn. 1998. Submicron structure in L-α-dipalmitoylphosphatidyl-choline monolayers and bilayers probed with confocal, atomic force, and near-field microscopy. *Biophys. J.* 75:342–353.
10. Nielsen, L. K., A. Vishnyakov, K. Jørgensen, T. Bjørnholm, and O. G. Mouritsen. 2000. Nanometre-scale structure of fluid lipid membranes. *J. Phys. Condens. Matter.* 12:A309–A314.
11. Cruz, A., L. Vázquez, M. Vélez, and J. Pérez-Gil. 2004. Effect of pulmonary surfactant protein SP-B on the micro- and nanostructure of phospholipid films. *Biophys. J.* 86:308–320.
12. Cruz, A., L. Vázquez, M. Vélez, and J. Pérez-Gil. 2005. Influence of a fluorescent probe on the nanostructure of phospholipid membranes: dipalmitoylphosphatidylcholine interfacial monolayers. *Langmuir.* 21:5349–5355.
13. Nielsen, L. K., T. Bjørnholm, and O. G. Mouritsen. 2007. Thermodynamic and real-space structural evidence of a 2D critical point in phospholipid monolayers. *Langmuir.* 23:11684–11692.
14. Keating, E., L. Rahman, J. Francis, A. Petersen, F. Possmayer, et al. 2007. Effect of cholesterol on the biophysical and physiological properties of a clinical pulmonary surfactant. *Biophys. J.* 93:1391–1401.
15. Coban, O., J. Popov, M. Burger, D. Vobornik, and L. J. Johnston. 2007. Transition from nanodomains to microdomains induced by exposure of lipid monolayers to air. *Biophys. J.* 92:2842–2853.
16. Zuo, Y. Y., E. Keating, L. Zhao, S. M. Tadayyon, R. A. W. Veldhuisen, et al. 2008. Atomic force microscopy studies of functional and dysfunctional pulmonary surfactant films. I. Micro- and nanostructures of functional pulmonary surfactant and the effect of SP-A. *Biophys. J.* 94:3549–3564.
17. Veatch, S. L., and S. L. Keller. 2005. Seeing spots: complex phase behavior in simple membranes. *c. Biochim. Biophys. Acta.* 1746:172–185.
18. London, E. 2005. How principles of domain formation in model membranes may explain ambiguities concerning lipid raft formation in cells. *Biochim. Biophys. Acta.* 1746.:203–220.
19. Kaganer, V. M., H. Möhwald, and P. Dutta. 1999. Structure and phase transitions in Langmuir monolayers. *Rev. Mod. Phys.* 71:779–819.
20. Scott, H. L. 2002. Modeling the lipid component of membranes. *Curr. Opin. Struct. Biol.* 12:495–502.
21. Venturoli, M., M. M. Sperotto, M. Kranenburg, and B. Smit. 2006. Mesoscopic models of biological membranes. *Phys. Rep.* 437:1–54.
22. Müller, M., K. Katsov, and M. Schick. 2006. Biological and synthetic membranes: what can be learned from a coarse-grained description? *Phys. Rep.* 434:113–176.
23. Laradji, M., and P. B. S. Kumar. 2005. Domain growth, budding, and fission in phase-separating self-assembled fluid bilayers. *J. Chem. Phys.* 123:224902.
24. Pandit, S. A., S. Vasudevan, S. W. Chiu, R. J. Mashl, E. Jakobsson, et al. 2004. Sphingomyelin-cholesterol domains in phospholipid membranes: atomistic simulation. *Biophys. J.* 87:1092–1100.
25. Shi, Q., and G. A. Voth. 2005. Multiscale modeling of phase separation in mixed lipid bilayers. *Biophys. J.* 89:2385–2394.
26. Illya, G., R. Lipowsky, and J. C. Shillcock. 2006. Effect of chain length and asymmetry on material properties of bilayer membranes. *J. Chem. Phys.* 125:114710.
27. Knecht, V., M. Müller, M. Bonn, S.-J. Marrink, and A. E. Mark. 2005. Simulation studies of pore and domain formation in a phospholipid monolayer. *J. Chem. Phys.* 122, 024704(1–9).
28. Wallace, E. J., N. M. Hooper, and P. D. Olmsted. 2005. The kinetics of phase separation in asymmetric membranes. *Biophys. J.* 88:4072–4083.
29. Frolov, V. A., Y. A. Chizmadziev, F. S. Cohen, and J. Zimmerberg. 2006. ''Entropic traps'' in the kinetics of phase separation in multicomponent membranes stabilize nanodomains. *Biophys. J.* 91:189–205.
30. Mikhailov, A., and G. Ertl. 1995. Pattern formation by adsorbates with attractive lateral interactions. *Chem. Phys. Lett.* 238:104–109.
31. Hildebrand, M., and A. S. Mikhailov. 1996. Mesoscopic modeling in the kinetic theory of adsorbates. *J. Phys. Chem.* 100:19089–19101.
32. Veldhuizen, R., K. Nag, S. Orgeig, and F. Possmayer. 1998. The role of lipids in pulmonary surfactant. *Biochim. Biophys. Acta.* 1408:90–108.
33. Hansen, J. P., and I. R. McDonald. 2006. Theory of Simple Liquids. Elsevier, Amsterdam.
34. Livadaru, L., and A. Kovalenko. 2004. Molecular description of the collapse of hydrophobic polymer chains in water. *J. Chem. Phys.* 121:4449–4452.
35. Livadaru, L., and A. Kovalenko. 2005. Self-consistent molecular theory of polymers in melts and solutions. *J. Phys. Chem. B.* 109:10631–10639.
36. Vaz, W. L., R. M. Clegg, and D. Hallmann. 1985. Translational diffusion of lipids in liquid crystalline phase phosphatidylcholine multilayers. A comparison of experiment with theory. *Biochemistry.* 24:781–786.

37. Filippov, A. G. O., and G. Lindblom. 2003. The effect of cholesterol on the lateral diffusion of phospholipids in oriented bilayers. *Biophys. J.* 84:3079–3086.

38. Orädd, G., P. W. Westerman, and G. Lindblom. 2005. Lateral diffusion coefficients of separate lipid species in a ternary raft-forming bilayer: a Pfg-NMR multinuclear study. *Biophys. J.* 89:315–320.

39. Deverall, M. A., E. Gindl, E.-K. Sinner, H. Besir, J. Ruehe, et al. 2005. Membrane lateral mobility obstructed by polymer-tethered lipids studied at the single molecule level. *Biophys. J.* 88:1875–1886.

40. Beglov, D., and B. Roux. 1995. Numerical solution of the hypernetted chain equation for a solute of arbitrary geometry in three dimensions. *J. Chem. Phys.* 103:360–364.

41. Kovalenko, A. 2003. Three-dimensional RISM theory for molecular liquids and solid-liquid interfaces. *In* Molecular Theory of Solvation. F. Hirata, editor. Kluwer Academic, Dordrecht, The Netherlands. 169–275.